Original Article

Investigation of Suitability of SST k-ω Turbulence Model with Low-Reynolds Number Correction for Impinging Jet Flow in Different Geometries and Thermal Boundary Conditions

S. Arslan[1], E. Pulat[2]

[1]Bursa Uludag University, Graduate School of Natural and Applied Science, Mechanical Engineering Department, Gorukle Campus, Nilufer, Bursa, Turkey
[2]Bursa Uludag University, Faculty of Engineering, Mechanical Engineering Department, Gorukle Campus, Nilufer, Bursa, Turkey

[1]*Corresponding Author : 512110006@ogr.uludag.edu.tr*

Abstract - Thermal jet flows are the type of flow frequently encountered in engineering applications. This article aims to determine if the SST k-ω turbulence model, including Low-Reynold Correction, accurately estimates the Nusselt number in impinging jet flow; because of this, computational results were compared with experimental studies. This comparison was made on a line (r/D) from stagnation point to exit. In this article, the heat transfer phenomenon in the impinging zone was observed computationally with the SST k-ω turbulence model on three impinging jet geometries with different boundary conditions using ANSYS FLUENT software. The boundary condition on the upper plate differs depending on whether there is confinement. The boundary condition on the impinging plate differs depending on whether there is a heat flux or fixed surface temperature. The flow type is a steady state. The software solver type is pressure-based because the flow velocity is too low compared to the local sound velocity.

1. Introduction

The impinging jet flow is frequently used in the industry due to its high heat and mass transfer. This method can achieve a high amount of heat and mass transfer, especially in the impinging area, by cooling or heating the gas or liquid fluid directed by the nozzle and impinging it on the surface.

Gopalakrishnan and Disimile (2018) validated the impinging jet flow at a constant Reynolds number at different angles. The results were very close to the experimental evidence with the SST k-ω model they used at 7500 Reynolds number and impinging angles of 30, 45, and 60 degrees, respectively. In addition, Gaussian dimensionless velocity profiles were also compatible with the experimental work in both the horizontal and vertical axis. Derdouri *et al.* (2019) computationally investigated the effect of cavity width on thermal behavior in round-impinging jet flow. The distance from the nozzle outlet to the impinging plate is taken as H=2D and Re=23000. The SST k-ω model was used to observe the turbulence effect. Veeranjaneyulu *et al.* (2018) investigated the effect of the impinging plate on jet flow in different material structures. SST k-ω was used as the turbulence model, and the Re number was taken as 5000, 10000, 15000, 20000, and 25000, respectively. Sinha and Raje (2021) investigated an anisotropic SST turbulence model for the boundary layer and compared a new SUQ-SST model with experimental studies. It is seen that the new model made improvements in predicting Reynold stress anisotropy and flow separation. Yu and Thé (2016) made validation for pollutant dispersion within a building array using SST k-ω as a turbulence model. They observed that the SST k-ω model is better than standard k-ε in predicting flow simulation. Garnayak and Patro (2020) investigated heat transfer from a small three-dimensional rectangular channel due to turbulent jet impinging. Numerical simulations were performed using the finite volume method with the SST k-ω turbulence model. They also compared the heat transfer enhancements with and without cross-flow effects and found that the heat transfer rate with cross-flow is higher than without cross-flow.

From the above studies, it can be seen that there are not enough studies in the literature about the SST k-ω turbulence model with low Reynolds correction despite studies including SST k-ω. In this study, the heat transfer phenomenon in the impinging zone was observed computationally with the SST k-ω turbulence model, including Low Reynolds Correction on three impinging jet geometries with different boundary conditions using ANSYS FLUENT software, and the analysis results were compared with the experimental studies in the literature.

2. Material and Method
2.1. Computational Method
There are two approaches to solving an engineering problem involving any fluid. These are the experimental approach and the computational approach. The first of these (experimental) usually requires a high cost and a long time in the application. For this reason, with the development of computer technology, less costly and less time-consuming computational methods have emerged than experimental studies. The use of computational methods, which are becoming popular in the industry daily, is based on computer algorithms and memory. Computational Fluid Dynamics (CFD), a particular interest in computational methods, has emerged mainly due to the complexity of engineering problems involving fluids. While computational fluid dynamics is generally used to validate experimental studies in academic studies, it is also used to solve many problems that arise in the industry. There are many commercial programs available today that use computational fluid dynamics. While preparing this study, ANSYS FLUENT commercial program was used.

2.2. SST k-ω Turbulence Model
Looking at the historical process, many 2-equation turbulence models have been proposed. (Pope, 2000) In these models, k is usually taken as the first variable, but the second variable differs. In homogeneous turbulence, the presence of the second variable is not essential, but the difference is in the diffusion term in non-homogeneous turbulence. With ω=ε/k, k, and ω are expressed by eq. (1) and eq. (2), respectively.

$$\frac{\partial(\rho k)}{\partial t} + \frac{\partial}{\partial x_j}\left[\rho u_j k - \left(\mu + \frac{\mu_t}{\sigma_k}\right)\frac{\partial k}{\partial x_j}\right]U_j\frac{\partial k}{\partial x_j} = \mu_t(P + P_B) - \rho\beta^* k\omega \qquad (1)$$

$$\frac{\partial(\rho\omega)}{\partial t} + \frac{\partial}{\partial x_j}\left[\rho u_j\omega - \left(\mu + \frac{\mu_t}{\sigma_\omega}\right)\frac{\partial\omega}{\partial x_j}\right] = \alpha\frac{\omega}{k}\mu_t P - \rho\beta\omega^2 + \rho S_\omega + C_{\varepsilon 3}\mu_t P_B C_\mu\omega \qquad (2)$$

2.3. Geometry
As the first geometry, van Heiningen *et al.* (2002) used the geometry they studied experimentally. As seen in Fig. 1a, the jet geometry is symmetrical, and the nozzle diameter is D=14.1 mm. The length of the impinging plate is 35.46D from the axis of symmetry to both sides, and the distance from the impinging plate to the nozzle exit is taken as H=2.6D.

As the second geometry, Del Frate *et al.* (2011) used the geometry they studied experimentally. As seen in Fig. 1b, the jet geometry is symmetrical, and the nozzle diameter is D=26 mm. The length of the impinging plate is 10D from the axis of symmetry to both sides, and the distance from the striker plate to the nozzle exit is taken as H=2D.

As the third geometry, Guerra *et al.* (2005) used the geometry they studied experimentally. As seen in Fig. 1c, the jet geometry is symmetrical, and the nozzle diameter is D=43.5 mm. The length of the impinging plate is 420 mm from the axis of symmetry to both sides, and the distance from the impinging plate to the nozzle exit is taken as H=2D.
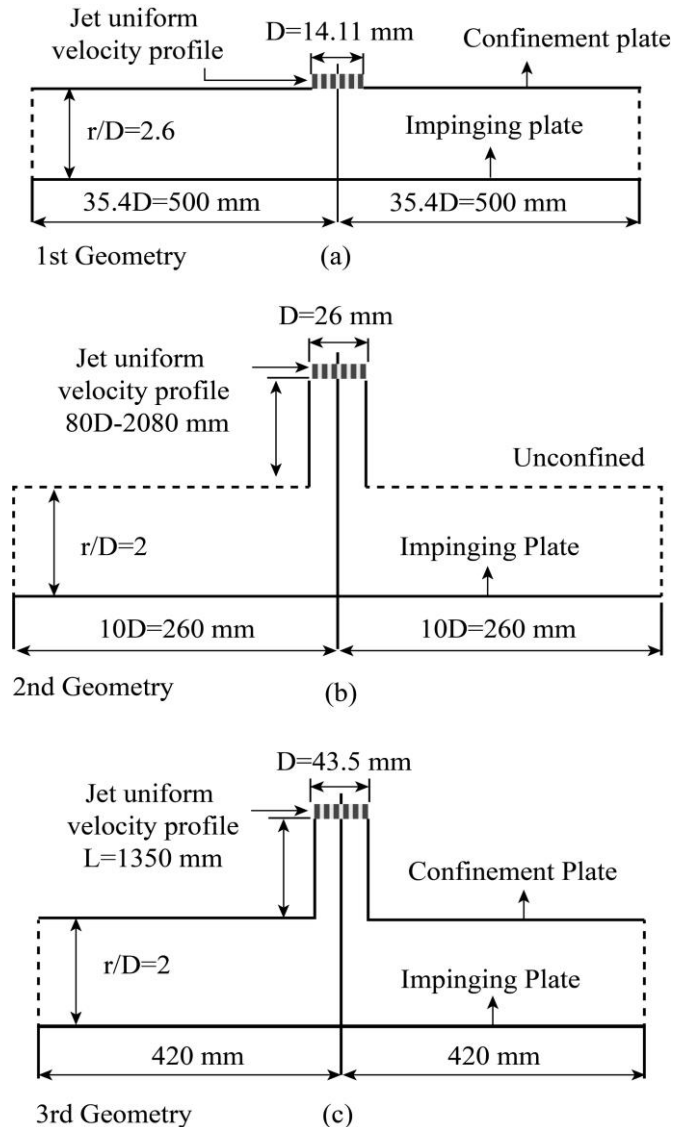
Fig. 1 Impinging jet geometries a) Confined b) Unconfined c) Confined

2.4. Boundary Conditions

The first geometry is the constrained jet with a constant surface temperature. As seen in Fig. 2a, air enters from the nozzle outlet at a temperature of 310 K and a speed of 12 m/s. The impinging plate is at a uniform temperature of 348 K; the limiting top plate is the fixed wall. The air outlet is to the atmosphere at atmospheric pressure.

The second geometry is the unconstrained (immersion) jet with constant heat flux. As seen in Fig. 2b, air enters the system from the nozzle exit at a temperature of 293 K and a speed of 13 m/s. The impinging plate is subjected to a uniform heat flux of 200 W/m², and the model does not have a limiting top plate. The air outlet is to the atmosphere at atmospheric pressure.

The third geometry is the constrained jet with constant heat flux. As seen in Fig. 2c, air enters the system from the nozzle exit at a temperature of 291.65 K and a speed of 12 m/s. The impinging plate is subjected to a uniform heat flux of 7000 W/m², and the limiting top plate is considered a fixed wall in the model. The air outlet is to the atmosphere at atmospheric pressure.

u, v = 0 (Noslip)   Tj = 310K   Uj = 12m / s   u, v = 0 (Noslip)

P=0   P=0

Ts = 348K

1st Geometry   (a)

Tj = 293K Uj = 13m / s

u, v = 0 (Noslip) P=0   u, v = 0 (Noslip) P=0

P=0   P=0

q=200W/m²

2nd Geometry   (b)

Tj = 291.65K Uj = 12m / s

u, v = 0 (Noslip)   u, v = 0 (Noslip)

P=0   P=0

q=7000 W/m²
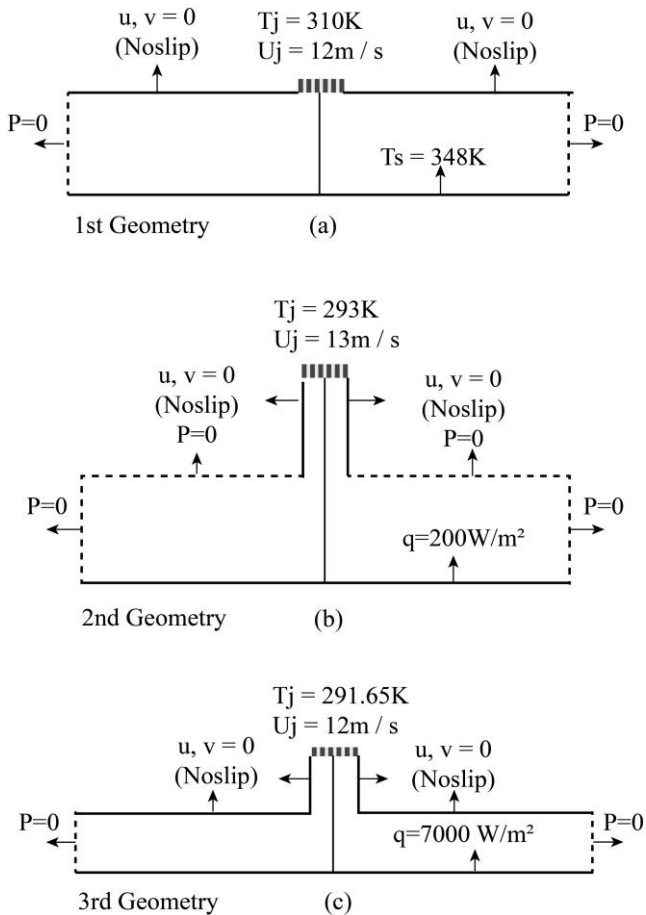
3rd Geometry   (c)

Fig. 2 Impinging jet boundary conditions a) Constant surface temperature b) Constant surface heat flux c) Constant surface temperature

The boundary conditions used are summarized in Table 1.

Table 1. Boundary xonditions used

1. Geometry	Confined	Constant Surface Temperature	(van Heiningen, 2002)
2. Geometry	Unconfined	Constant Heat Flux	(Del Frate, 2011)
3. Geometry	Confined	Constant Heat Flux	(Guerra, 2005)

3. Results and Discussion

3.1. The Geometry which is Confined and has Constant Surface Temperature

The y+ values in different mesh sizes in the SST k-ω model of the van Heiningen geometry are shown in Fig. 3.
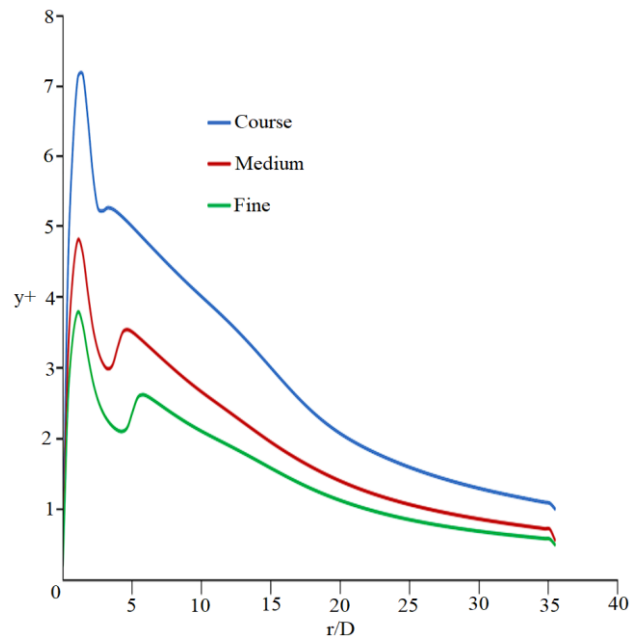
Fig. 3 Comparison of y⁺ value in different mesh sizes as a chart

The y+ values in different mesh sizes in the SST k-ω model of van Heiningen geometry are shown in Table 2.

Table 2. Comparison of y⁺ value in different mesh sizes

	Max y+	Min y+	Average y+
Course	7.2	0.5	2.9
Medium	4.8	0.3	1.9
Fine	3.8	0.2	1.5

While the lower surface has a constant temperature of 348 K in the van Heiningen geometry when the air jet outlet temperature is taken as 286 K, the Nusselt number is lower than the experimental result in the SST k-ω model at the stagnation point, as seen in fig. 4. Different mesh sizes do not differ significantly. The results are close to the experimental study from just after the stagnation point along the impinging surface. In the range 0 < r/D < 5, the value of the secondary

peak is lower than in the experimental study but occurs approximately between 4 < r/D < 6.
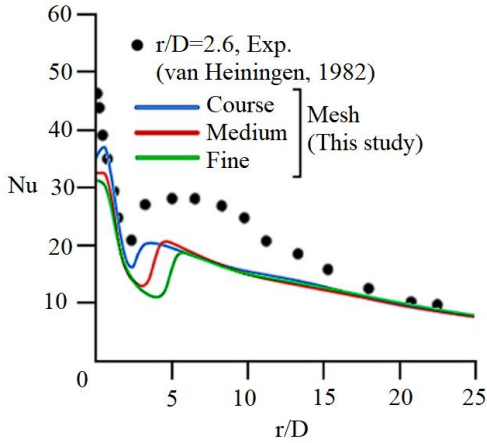
Fig. 4 Comparison SST k- ω turbulence model, which has low-Reynold correction with experiment study in the van Heiningen geometry

While the lower surface has a constant temperature of 348 K in van Heiningen geometry when the air jet outlet temperature is taken as 310 K, the Nusselt number is slightly higher than the experimental result in the SST k-ω model at the stagnation point, as seen in fig. 5. There was no significant difference in different network structures. The results are close to the experimental work from just after the stagnation point along the imping surface. The value of the secondary peak in the range 0 < r/D < 5 is close to the experimental study but occurs approximately between 4 < r/D < 6.
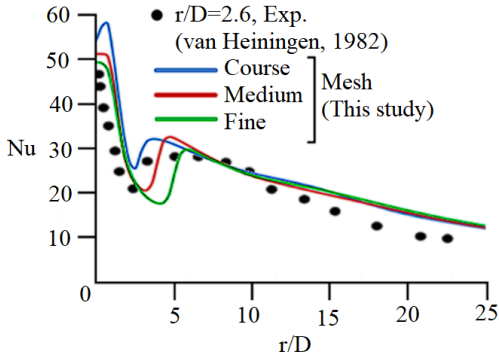
Fig. 5 Comparison SST k-ω turbulence model, which has low-Reynolds correction with experimental study in the van Heiningen geometry

3.2. The Geometry which is Unconfined and has Constant Heat Flux

The y+ values in different mesh sizes in the SST k-ω model of Del Frate geometry are shown in fig. 6.

The comparison of the minimum, maximum and average y+ values in different mesh sizes in the SST k-ω model of Del Frate geometry is shown in Table 3.
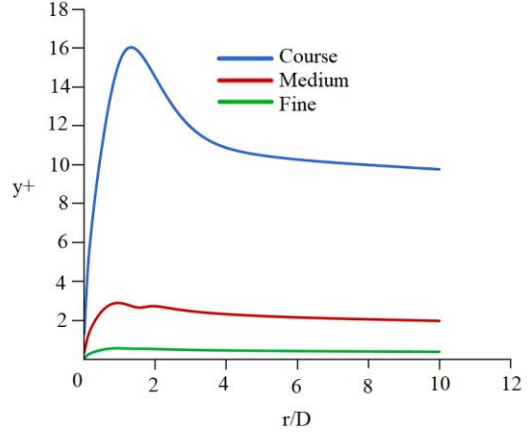
Fig. 6 Comparison of y+ value in different mesh sizes as a chart

Table 3. Comparison of y+ value in different mesh sizes

	Max y+	Min y+	Average y+
Course	16	1.3	11.1
Medium	2.9	0.3	2.2
Fine	0.6	0	0.4

While the bottom surface has a constant heat flux of 200 W/m^2 in Del Frate geometry, when the air jet outlet temperature is taken as 293.55 K, the Nusselt number has the same value as the experimental result in the SST k-ω model at the stagnation point, as seen in figure 7. From the point of rest along the imping surface, close results are obtained with the experimental study. In the range 0 < r/D < 2, the value of the secondary peak occurs close to the experimental study but occurs at approximately r/D=2.
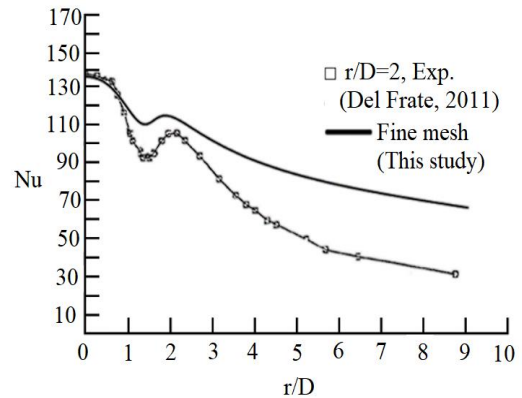
Fig. 7 Comparison SST k-ω turbulence model, which has low-Reynolds correction with experimental study in the Del Frate geometry

3.3. The Geometry which is Confined and has Constant Heat Flux

The y+ values in fine mesh sizes in the SST k-ω model of Guerra geometry are shown in Figure 8.
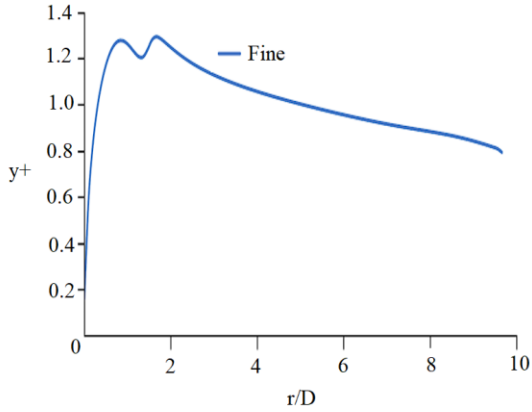
Fig. 8 Comparison of y+ value in different mesh sizes as a chart

The comparison of the minimum, maximum and average y+ values in Fine mesh structures in the SST k-ω model of Guerra geometry is shown in Table 4.

Table 4. Comparison of y^+ value in fine mesh size

	Max y^+	**Min y^+**	**Average y^+**
Fine	1.3	0.16	1.01

While the lower surface has a constant heat flux of 7000 W/m^2 in Guerra geometry, when the air jet outlet temperature is taken as 291.65 K, the Nusselt number in the SST k-ω model at the stagnation point is much higher than the experimental result, as shown in Figure 9a. The secondary peak along the impinging surface occurs around 2 < r/D < 3.

As shown in Figure 9a, the Nusselt number value and graphic trend differ with changing turbulence intensity on the second peak. When turbulence intensity is taken %2 based on Figure 9a, changing of Nusselt number with different length scales has seen in Figure 9b. A %2 turbulence intensity inlet length scale of 0.005 has shown the best compatibility with the experimental result.

4. Conclusion

It has been observed that different mesh sizes do not make a significant difference in the confined geometry (van Heiningen geometry) with constant surface temperature. In addition, it has been observed that the jet exit temperature increased the Nusselt number in the impinging region.

It has been observed that the numerical values are very close to the experimental values in the unconfined geometry (Del Frate geometry) with constant heat flux.

It has been observed that although the numerical values are far from the experimental values at the stagnation point, as from r/D>0, numerical values are close to experimental values in the confined geometry (Guerra geometry) with constant heat flux. In addition, it has been observed that although inaccuracy in stagnation point, with %2 inlet turbulence intensity 0.005 m length scale showed a better trend on second peak estimation.

It is known from the studies in the literature that the SST k-ω model is successful in impinging jet flow. In this study, it has been observed that the SST k-ω model gives more accurate results with Low Reynold correction in impinging jet flow.
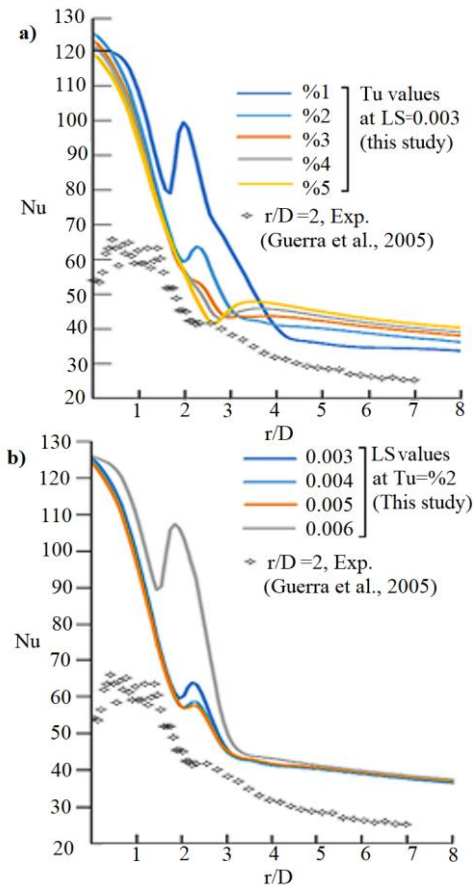
Fig. 9 Comparison SST k- ω turbulence model with experimental values a) Effect of turbulence intensity (LS=0.003)   b) Effect of length scale (Tu=%2)

References

[1] Sedat Arslan, and Erthan Pulat, "Modification of Model Constants for Two-Equation Turbulence Models in Impinging Jet Thermoflows," *Euroasia Journal of Mathematics, Engineering, Natural & Medical Science*, vol.25, no. 2, pp. 22-36, 2022. [Google Scholar] [Publisher Link]

[2] L. Del Frate et al., "CFD Simulations of a Normally-Impinging Jet from a Circular Nozzle," *20th International Conference Nuclear Energy for New Europe*, 2011. [Google Scholar] [Publisher Link]

[3] Derdouri et al., "Numerical Study of a Round Jet İmpinging on an Axisymmetric Grooved Surface: Effect of the Groove Size," *Thermophysics and Aeromechanics*, vol. 27, no. 5, pp. 671-690, 2019. [CrossRef] [Google Scholar] [Publisher Link]

[4] Uriel C. Goldberg, and Paul Batten, "A Wall Distance Free Version of the SST Turbulence Model," *Engineering Applications of Computational Fluid Mechanics*, vol. 9, no. 1, pp. 33-40, 2015. [CrossRef] [Google Scholar] [Publisher Link]

[5] Raj Narayan Gopalakrishnan, and Peter J. Disimile, "CFD Analysis of Twin Turbulent Impinging Round Jets at Different Impingement Angles," *Fluids*, vol. 3, no. 4, 2018. [CrossRef] [Google Scholar] [Publisher Link]

[6] Danielle R.S. Guerra, Jian Su, and Atila P. Silva Freire, "The Near Wall Behavior of an İmpinging Jet," *International Journal of Heat and Mass Transfer*, vol. 48, no. 14, pp. 2829-2840, 2005. [CrossRef] [Google Scholar] [Publisher Link]

[7] J. E. Jaramillo et al., "Analysis of different RANS Models Applied to Turbulent Forced Convection," *International Journal of Heat and Mass Transfer*, vol. 50, no. 19-20, pp. 3749-3766, 2007. [CrossRef] [Google Scholar] [Publisher Link]

[8] William P. Klinzing, and Ephraim M. Sparrow, "Evaluation of Turbulence Models for External Flows," *Numerical Heat Transfer*, *Part A: Applications*, vol. 55, no. 3, pp. 205-228, 2009. [CrossRef] [Google Scholar] [Publisher Link]

[9] Konstantin Kurbatskii, "Comparison of RANS Turbulence Models in Numerical Prediction of Chevron Nozzle Jet Flows," *Aerospace Research Cemtral*, 2009. [CrossRef] [Google Scholar] [Publisher Link]

[10] Babak Yousefi-Lafouraki, Abas Ramiar, and Ali Akbar Ranjbar, "Numerical Simulation of Two Phase Turbulent Flow of Nanofluids in Confined Slot Impinging Jet," *Flow, Turbulent and Combust,* vol. 97, pp. 571-589, 2016. [CrossRef] [Google Scholar] [Publisher Link]

[11] S. H. Lam, "On the RNG Theory of Turbulence," *Physics of Fluids*, vol. 4, no. 5, pp. 1007-1017, 1992. [CrossRef] [Google Scholar] [Publisher Link]

[12] D. H. Lee, Y. S. Chung, and D. S. Kim, "Turbulent Flow and Heat Transfer Measurements on a Curved Surface with Fully Developed Round İmpinging Jet," *International Journal of Heat and Fluid Flow*, vol. 18, no. 1, pp. 160-169, 1997. [CrossRef] [Google Scholar] [Publisher Link]

[13] P. Majumdar, *Computational Fluid Dynamics and Heat Transfer*, CRC Press, New York, 2022.

[14] Amir H. Ghahremani, and Reza Saleh, "Numerical Study of Turbulence Models in heat Transfer of a Confined and Submerged Jet Impingement using AL2O3 - Water Nano Fluid," *SSRG International Journal of Mechanical Engineering*, vol. 2, no. 5, pp. 47-55, 2015. [CrossRef] [Google cholar] [Publisher Link]

[15] Holger Martin, "Heat and Mass Transfer between Impinging Gas Jets and Solid Surfaces," *Advances in Heat Transfer,* vol. 13, pp. 1-60, 1977. [CrossRef] [Google Scholar] [Publisher Link]

[16] M. Molana, and S. Banooni, "Investıgatıon of Heat Transfer Processes Involved Liquıd Impıngement Jets: A Revıew*," Brazilian journal of Chemical Engineering*, vol. 30, no. 3, pp. 413-435, 2013. [CrossRef] [Google Scholar] [Publisher Link]

[17] Mohammad Moshfeghi, Ya Jun Song, and Yong Hui Xie, "Effects of Near-Wall Grid Spacing on SST k-ω Model Using NREL Phase VI Horizontal Axis Wind Turbine," *Journal of Wing Engineering and Industrial Aerodynamics*, vol. 107-108, pp. 94-105, 2012. [CrossRef] [Google Scholar] [Publisher Link]

[18] P. Patro, and S. Garnayak, "Heat Transfer Enhancement from a Heated Plate with Hemispherical Convex Dimples by Forced Convection along with a Cross Flow Jet Impingement," *International Journal of Applied Mechanics and Engineering*, vol. 25, no. 1, pp. 127-141, 2020. [CrossRef] [Google Scholar] [Publisher Link]

[19] Nishant Kumar, Saurav Upadhaya, Ashish Rohilla, "Evaluation of the Turbulence Models for the Simulation of the flow over a Tsentralniy Aerogidrodinamicheskey Institut (TsAGI)-12% Airfoil," *SSRG International Journal of Mechanical Engineering*, vol. 4, no. 1, pp. 18-28, 2017. [CrossRef] [Google Scholar] [Publisher Link]

[20] S.B. Pope, *Turbulent Flow*, Cambridge University Press, 2000. [Google Scholar]

[21] U. Rohde et al., "Fluid Mixing and flow Distribution in a Primary Circuit of a Nuclear Pressurized Water Reactor—Validation of CFD Codes," *Nuclear Engineering and Design*, vol.237, no. 15-17, pp. 1639-1655, 2007. [CrossRef] [Google Scholar] [Publisher Link]

[22] Hassan Raiesi, Ugo Piomelli, and Andrew Pollard, "Evaluation of Turbulence Models Using Direct Numerical and Large-Eddy Simulation Data," *Journal of Fluids Engineering*, vol. 133, no. 2, 2011. [CrossRef] [Google Scholar] [Publisher Link]

[23] Pratikkumar Raje, and Krishnendu Sinha, "Anisotropic SST Turbulence Model for Shock-Boundary Layer Interaction," *Computers & Fluids*, vol. 228, 2021. [CrossRef] [Google Scholar] [Publisher Link]

[24] Y. Shi, M. B. Ray, and A. S. Mujumbar, "Computational Study of Impingement Heat Transfer under a Turbulent Slot Jet," *Industrial & Engineering Chemistry Research*, vol. 41, no. 18, pp. 4643-4653, 2002. [CrossRef] [Google Scholar] [Publisher Link]

[25] Hemal Lakdawala et al., "Experimental Investigations of Jet Expansion for Hydraulic Nozzles of Different Materials," *International Journal of Engineering Trends and Technology,* vol. 70, no. 3, pp. 140-150, 2022. [CrossRef] [Publisher Link]

[26] M. Shur, and P. R. Spalart, "On the Sensitization of Turbulence Models to Rotation and Curvature," *Aerospace Science and Technology*, vol. 5, pp. 297-302, 1996. [CrossRef] [Google Scholar] [Publisher Link]

[27] Versteeg Henk Kaarle, and Weeratunge Malalasekera, *An İntroduction to Computational Fluid Dynamics: The Finite Volume Method*, Pearson Education, 2007. [Google Scholar]

[28] Peng Wang et al., "Numerical İnvestigation of the Flow and Heat Behaviours of an İmpinging Jet," *International Journal of Computational Fluid Dynamics*, vol. 28, pp. 301-315, 2014. [CrossRef] [Google Scholar] [Publisher Link]

[29] Micha Wolfshtein, "Some Comments on Turbulence Modelling," *International Journal of Heat and Mass Transfer*, vol. 52, no. 17-18, pp. 4103-4107, 2009. [CrossRef] [Google Scholar] [Publisher Link]

[30] Ming Wu, "Numerical Calculation of Hydrodynamics for UUV Based on SST Turbulence Model," *7th International Conference on Intelligent Human-Machine Systems and Cybernetics*, pp. 424-427, 2015. [CrossRef] [Google Scholar] [Publisher Link]

[31] Hesheng Yu, and Jesse The, "Validation and Optimization of SST k- ω Turbulence Model for Pollutant Dispersion within a Building Array," *Atmospheric Environment*, vol. 145, pp. 225-238, 2016. [CrossRef] [Google Scholar] [Publisher Link]